CCD Photometry, Period Analysis, and Evolutionary Status of the Pulsating Variable V544 Andromedae

Kevin B. Alton
UnderOak and Desert Bloom Observatories, 70 Summit Ave, Cedar Knolls, NJ 07927; kbalton@optonline.net

Received October 7, 2019; revised November 15, 2019; accepted November 20, 2019

Abstract Multi-color (BVR_c) CCD-derived photometric data were acquired from V544 And, a pulsating variable presently classified as an SX Phe-type subdwarf system. Deconvolution of time-series light curve (LC) data was accomplished using discrete Fourier transformation and revealed a mean fundamental mode (f_0) of oscillation at 9.352 d^{-1} along with five other partial harmonics ($2f_0$–$6f_0$). No other statistically significant frequency shared by all bandpasses was resolved. Potential secular period changes were evaluated using four new times-of-maximum (ToMax) light produced from the present study along with other values reported in the literature. In addition, photometric data collected during the SuperWASP (2006–2007) survey combined with CCD-derived V-mag data acquired from the AAVSO archives produced twenty-nine more ToMax measurements. Corresponding residuals from the observed minus calculated values indicate very little change in the primary pulsation period since 2004. The evolutionary status, age, and physical nature of V544 And were investigated using the PAdova and TRieste Stellar Evolution Code (PARSEC) for generating stellar tracks and isochrones. At this time, the weight of evidence points to a HADS rather than an SX Phe-type pulsating star.

1. Introduction

High amplitude δ Scuti stars, hereafter HADS, represent less than 1% of all δ Sct variables (Lee *et al.* 2008). They commonly oscillate via low-order single or double radial pulsation modes (Poretti 2003a, 2003b; Niu *et al.* 2013, 2017). Pulsations are driven by the κ-mechanism resulting from partial ionization of He II (Pamyatnykh *et al.* 2004). Many (~40%) are double pulsators showing simultaneous pulsations in the fundamental and the first overtone mode with amplitudes generally higher in the fundamental mode (McNamara 2000). Non-radial pulsations have also been detected with the HADS variable V974 Oph (Poretti 2003a, 2003b). HADS variables have historically been divided according to metallicity relative to the Sun ([Fe/H] = 0). The metal-poor ([Fe/H] << 0) group has been traditionally classified as SX Phe-type variables based on the prototype SX Phoencis. Purportedly they have shorter periods ($0.02 < P < 0.125$ d) and lower masses (~1.0–1.3 $M_\odot$) than their sibling HADS variables possessing near solar metal abundance (McNamara 2011). SX Phe stars frequently reside in globular clusters (GC) which are ancient collections of Population II stars. Therein, the majority of SX Phe variables are classified as blue straggler stars, paradoxically appearing much younger than their GC cohorts. Balona and Nemec (2012) proposed that it is not possible to differentiate between δ Sct and field SX Phe variables based on pulsation amplitude, the number of pulsation modes, period, or even metallicity (Garg *et al.* 2010). Much more sensitive space telescopes like Kepler (Gilliland *et al.* 2010), CoRoT (Baglin 2003), and MOST (Walker *et al.* 2003) have found many examples that contradict these historically accepted definitions. They further contend that the evolutionary status of each star is the only way to distinguish between these two classes.

The variability of V544 Andromedae (GSC 02815-00790) was first identified from an evaluation of unfiltered photometric data collected during the ROTSE-I Survey (Akerlof *et al.* 2000; Wozniak *et al.* 2004). Khruslov (2008) reported that V544 And (NSVS 3844113, NSVS 6459386, and NSVS 6472319) was an SX Phe-type variable with a period of 0.10694 d. Photometric (V-mag) data from V544 And were downloaded from the AAVSO International Database (Kafka 2019). Herein, an assessment of these and other LC data from the SuperWASP Survey (Butters *et al.* 2010) further confirmed the fundamental period reported by Khruslov (2008). This report marks the first multi-color photometric study on V544 And which also critically assesses its previous classification as an SX Phe-type pulsator.

2. Observations and data reduction

2.1. Photometry

Time-series images were acquired at Desert Blooms Observatory (DBO; 110.257 W, 31.941 N) with an SBIG STT-1603ME CCD camera mounted at the Cassegrain focus of a 0.4-m ACF-Cassegrain telescope. This telecompressed (0.62 ×) f/6.8 instrument produced an image scale of 1.36 arcsec/pixel (bin = 2 × 2) and a field-of-view (FOV) of 17.2' × 11.5'. Image acquisition (75-s) was performed using THESKYX PRO Version 10.5.0 (Software Bisque 2019). The CCD-camera is equipped with B, V, and R_c filters manufactured to match the Johnson-Cousins Bessell specification. Dark subtraction, flat correction, and registration of all images collected at DBO were performed with AIP4WIN v2.4.0 (Berry and Burnell 2005). Instrumental readings were reduced to catalog-based magnitudes using the MPOSC3 star fields (Warner 2007) built into MPO CANOPUS v10.7.1.3 (Minor Planet Observer 2019). Light curves (LC) for V544 And were generated using an ensemble of five non-varying comparison stars. The identity, J2000 coordinates, and MPOSC3 color indices (B–V) for these stars are provided in Table 1. A representative image containing the target (T) and matching ensemble of comparison stars (1–5) is also provided (Figure 1). Data from images taken below 30° altitude (airmass > 2.0) were excluded; considering the proximity of all program stars, differential atmospheric extinction was ignored. During each imaging session comparison stars typically stayed within ± 0.009 mag for V and R_c filters and ± 0.015 mag for B passband.

Table 1. Astrometric coordinates (J2000), V-mag, and color indices (*B–V*) for V544 And and five comparison stars (1–5) used during this photometric study.

FOV ID	*Star Identification*	*R.A. h m s*	*Dec. ° m s*	*MPOSC3[a] V-mag*	*MPOSC3[a] (*B–V*)*
T	V544 And[b]	01 44 27.968	+37 58 53.697	12.790	0.231
1	GSC 02815-01525	01 44 44.500	+38 02 06.345	11.082	0.385
2	GSC 02815-01590	01 44 49.205	+38 02 27.708	13.298	0.531
3	GSC 02815-01205	01 45 00.547	+38 05 22.596	11.709	0.623
4	GSC 02815-00872	01 44 07.721	+38 01 57.396	13.066	0.572
5	GSC 02815-01467	01 44 44.597	+38 02 54.960	13.543	0.683

[a] *V-mag and (*B–V*) for comparison stars derived from* MPOSC3 *database described by Warner (2007).*
[b] *Mean V-mag and (*B–V*) determined during this study.*

Table 2. Times of maximum (ToMax), measurement uncertainty, filter type, epoch, and fundamental pulsation timing differences (PTD) for V544 And used to calculate a new linear ephemeris.

ToMax (HJD–2400000)	*Uncertainty*	*Filter[a]*	*Cycle No.*	*PTD*	*Ref.*	*ToMax (HJD–2400000)*	*Uncertainty*	*Filter[a]*	*Cycle No.*	*PTD*	*Ref.*
53201.6971	0.0011	T	–49048	–0.0011	1	56587.3408	0.0005	C	–17388	–0.0005	6
53220.6268	0.0014	T	–48871	0.0007	1	56587.4482	0.0004	C	–17387	0.0000	6
53228.6461	0.0007	T	–48796	–0.0004	1	56587.5549	0.0003	C	–17386	–0.0002	6
53229.6101	0.0016	T	–48787	0.0011	1	56920.3443	0.0035	TG	–14274	–0.0005	7
53232.6039	0.0021	T	–48759	0.0007	1	56920.3443	0.0035	TR	–14274	–0.0005	7
53235.5976	0.0013	T	–48731	0.0002	1	56920.3445	0.0035	TB	–14274	–0.0003	7
53238.5923	0.0013	T	–48703	0.0006	1	56920.4507	0.0035	TG	–14273	–0.0010	7
53241.5851	0.0015	T	–48675	–0.0008	1	56920.4509	0.0035	TR	–14273	–0.0008	7
53241.6918	0.0014	T	–48674	–0.0011	1	56920.4513	0.0035	TB	–14273	–0.0004	7
53245.6504	0.0016	T	–48637	0.0008	1	56928.3646	0.0010	C	–14199	–0.0005	8
53256.5579	0.0018	T	–48535	0.0007	1	56928.4713	0.0005	C	–14198	–0.0008	8
53256.6635	0.0011	T	–48534	–0.0006	1	56970.2481	0.0015	0	–13807.5[b]	0.0169	7
54049.3928	0.0016	T	–41121	0.0006	1	56970.3565	0.0013	0	–13806.5[b]	0.0184	7
54049.6064	0.0012	T	–41119	0.0002	1	57004.2907	0.0006	V	–13489	–0.0001	8
54103.3948	0.0016	T	–40616	–0.0009	1	57004.3981	0.0009	V	–13488	0.0004	2
55117.3794	0.0014	V	–31134	0.0018	2	57004.3983	0.0008	V	–13488	0.0006	8
55117.4861	0.0016	V	–31133	0.0016	2	57294.4125	0.0009	V	–10776	0.0001	2
55117.5923	0.0012	V	–31132	0.0008	2	57294.5182	0.0008	V	–10775	–0.0011	2
55227.3092	0.0009	V	–30106	–0.0002	2	57667.3050	0.0008	V	–7289	0.0014	2
55227.4153	0.0008	V	–30105	–0.0010	2	57727.2963	0.0008	V	–6728	0.0007	2
55452.4119	0.0007	V	–28001	–0.0011	3	58104.3571	0.0007	V	–3202	–0.0004	2
55452.5192	0.0006	V	–28000	–0.0007	3	58177.2880	0.0007	V	–2520	–0.0008	2
55452.6263	0.0005	V	–27999	–0.0005	3	58384.6407	0.0007	V	–581	–0.0001	2
55531.4399	0.0005	V	–27262	0.0001	3	58443.6707	0.0010	R_c	–29	0.0004	9
55851.2895	0.0004	C	–24271	–0.0006	4	58443.6711	0.0012	B	–29	0.0008	9
55870.2183	0.0006	V	–24094	0.0003	4	58443.6715	0.0011	V	–29	0.0012	9
55870.3251	0.0004	V	–24093	0.0002	4	58443.7765	0.0005	R_c	–28	–0.0007	9
55870.4321	0.0004	V	–24092	0.0002	4	58443.7775	0.0004	V	–28	0.0002	9
55870.5389	0.0005	V	–24091	0.0001	4	58443.7785	0.0016	B	–28	0.0013	9
56228.3511	0.0007	V	–20745	–0.0008	5	58446.6635	0.0011	R_c	–1	–0.0010	9
56228.3521	0.0010	V	–20745	0.0002	2	58446.6647	0.001	V	–1	0.0001	9
56235.3026	0.0014	C	–20680	–0.0002	5	58446.6656	0.0014	B	–1	0.0011	9
56581.2459	0.0012	C	–17445	0.0001	6	58446.7703	0.0013	R_c	0	–0.0012	9
56581.3541	0.0008	C	–17444	0.0014	6	58446.7712	0.0014	V	0	–0.0003	9
56587.2341	0.0005	C	–17389	–0.0002	6	58446.7724	0.0018	B	0	0.0009	9

[a] *T = TAMMAG2 from SuperWASP; C = clear; 0 = no filter; TG = tricolor green channel; TR = tricolor red channnel; TB = tricolor blue channel; V, B, and* R_c *= photometric Johnson-Cousins.*

[b] *Anomalous values not used for determination of linear ephemeris.*

Reference note: 1. SuperWASP: Butters et al. *(2010); 2. AAVSO International Variable Star Index: Watson* et al. *(2014); 3. Wils* et al. *(2011); 4. Wils* et al. *(2012); 5. Wils* et al. *(2013); 6. Wils* et al. *(2014); 7. Hűbscher (2015); 8. Wils* et al. *(2015); 9. This study at DBO.*

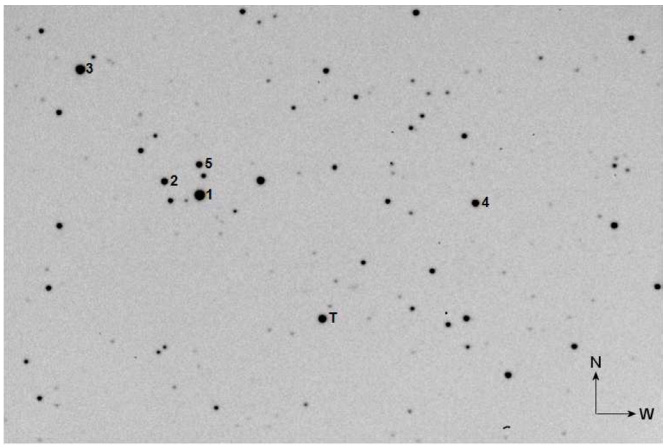

Figure 1. FOV (17.2 × 11.5 arcmin) containing V544 And (T) along with the five comparison stars (1–5) used to reduce time-series images to MPOSC3-catalog based magnitudes.

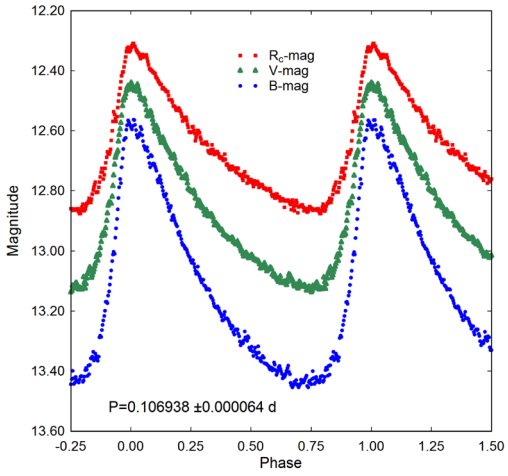

Figure 2. Period folded (0.106938 ± 0.000064 d) LCs for V544 And produced from photometric data obtained between 21 Nov and 24 Nov 2018, at DBO. LCs shown at the top (R_c), middle (V,) and bottom (B) represent catalog-based (MPOSC3) magnitudes determined using MPO CANOPUS.

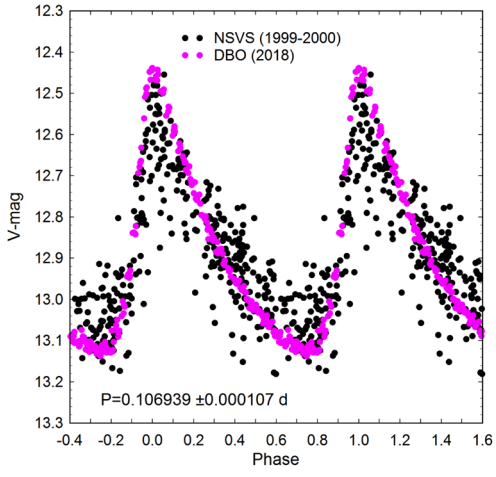

Figure 3. Period folded (0.106939 ± 0.000107 d) LCs for V544 And produced with sparsely sampled data from the ROTSE-I (1999–2000) Survey. Precise time-series V-mag data acquired at DBO (2018) are superimposed for direct comparison with ROTSE-I magnitudes which have been offset to conform to the DBO-derived V-mag values.

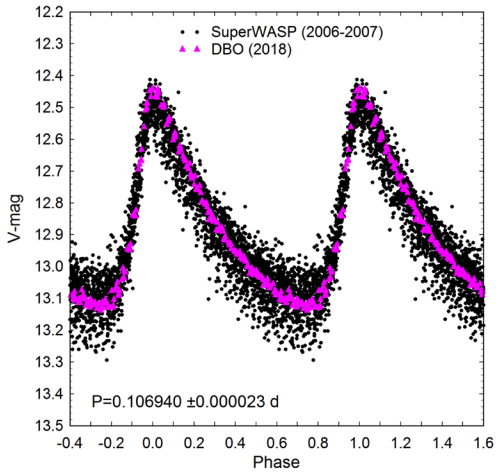

Figure 4. Period folded (0.106940 ± 0.000023 d) LCs for V544 And produced with broad-band (400–700 nm) filtered data from the SuperWASP survey (2006–2007). Precise time-series V-mag data acquired at DBO (2018) are superimposed for direct comparison with SuperWASP magnitudes which have been offset to conform to the DBO-derived V-mag values.

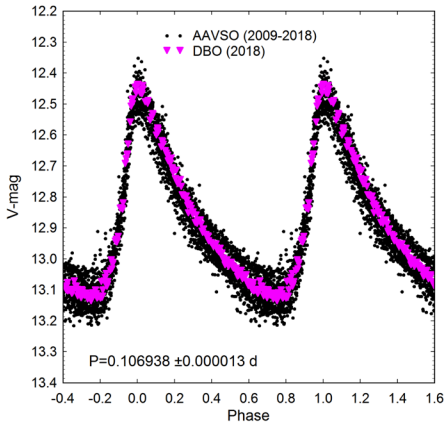

Figure 5. Period folded (0.106938 ± 0.000013 d) LCs for V544 And produced with V-mag data from the AAVSO archives (2009–2018). Precise time-series V-mag data acquired at DBO (2018) are superimposed for direct comparison with the AAVSO data which have been offset to conform to the DBO-derived V-mag values.

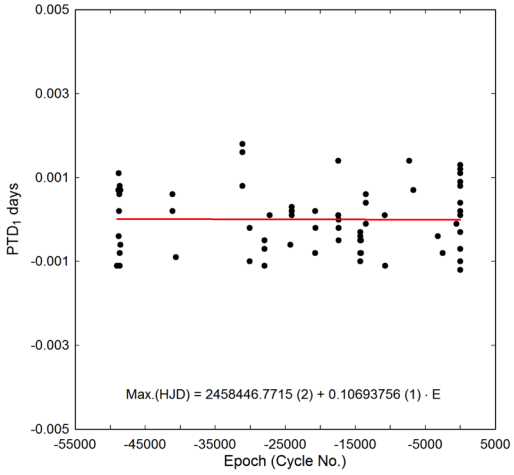

Figure 6. Straight line fit of pulsation timing difference vs. period cycle number indicating overall little or no change to the fundamental pulsation period of V544 And had occurred between 2004 and 2018.

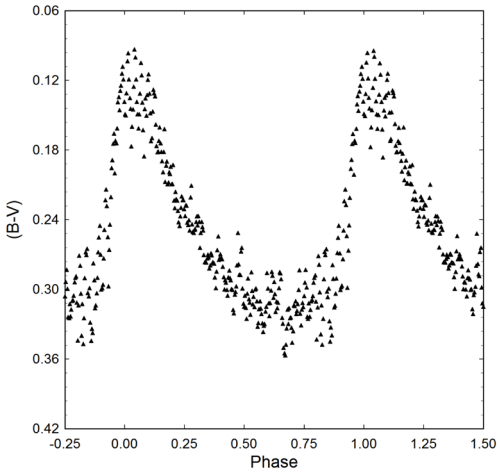

Figure 7. V544 And LC illustrating significant increase in reddening ($0.136 < (B–V) < 0.326$) as maximum light slowly descends to minimum light. This effect is most closely associated with a decrease in the effective surface temperature during minimum light.

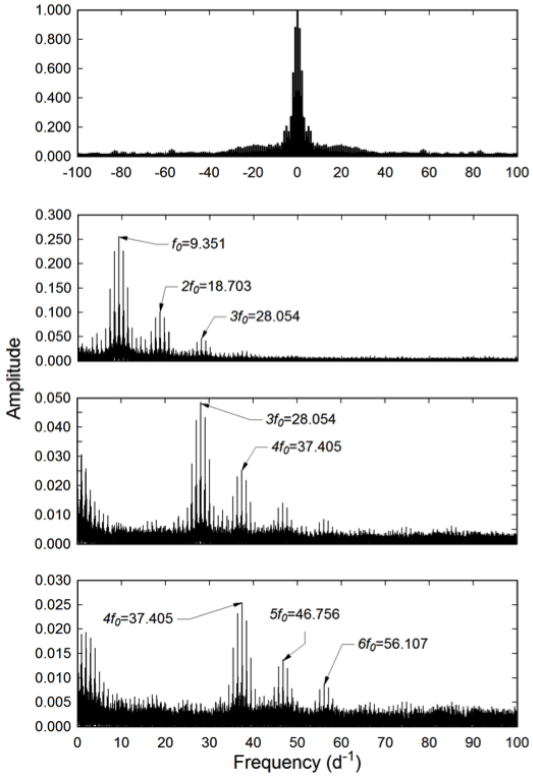

Figure 8. Amplitude spectra showing spectral window (top) and all significant pulsation frequencies following DFT analysis of photometric data from V544 And acquired by the SuperWASP survey between 21 Aug 2006 and 03 Jan 2007. This includes the fundamental f_0 frequency through its highest partial harmonic $6f_0$ detected ($S/N \geq 6$) following prewhitening.

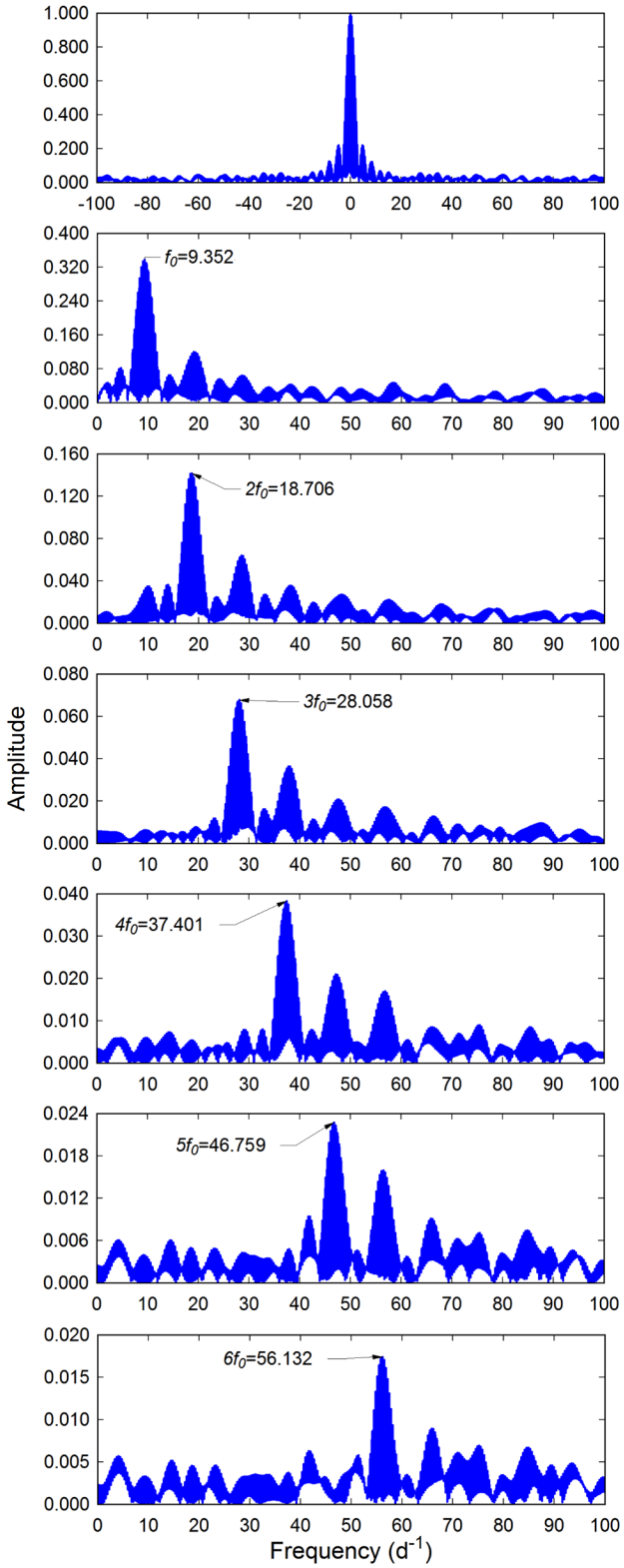

Figure 9. Amplitude spectra showing all significant pulsation frequencies following DFT analysis of B-mag photometric data from V544 And acquired at DBO between 21 Nov and 24 Nov 2018. This includes the spectral window (top) and the fundamental f_0 frequency through its highest partial harmonic $6f_0$ detected ($S/N \geq 6$) following prewhitening.

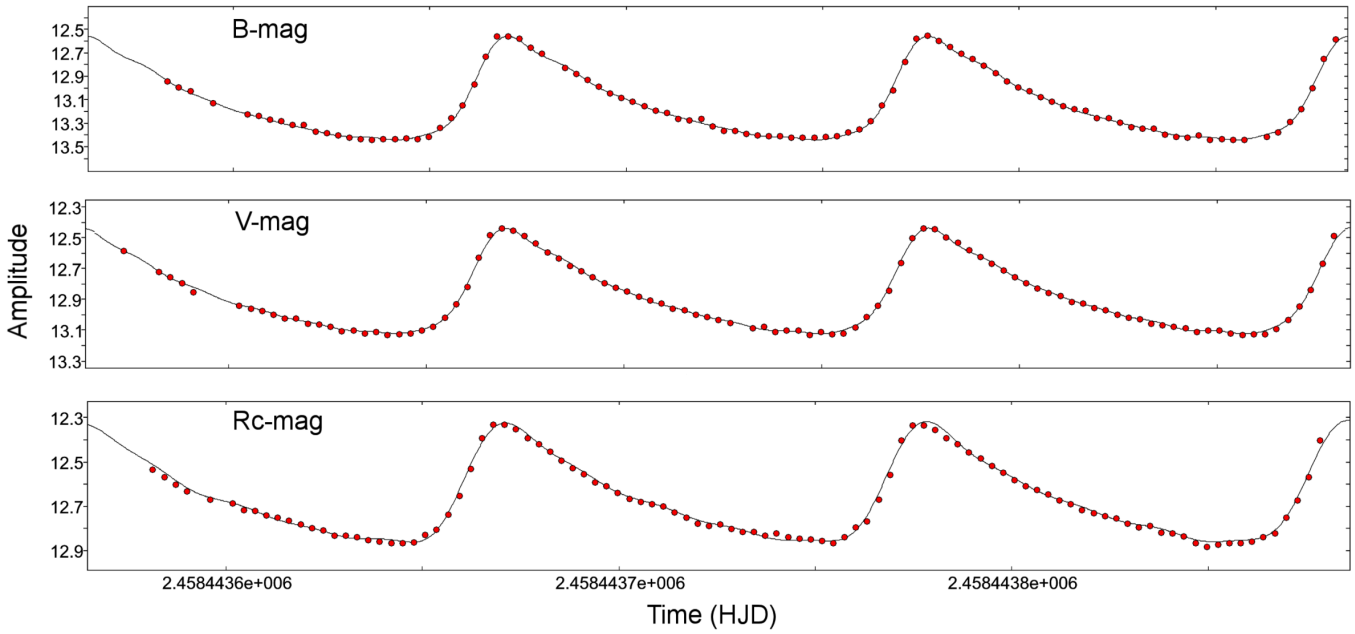

Figure 10. Representative DFT fit of B- (top), V- (middle), and R_c-mag (bottom) time series data based on elements derived from DFT. These data were acquired on 21 Nov 2018 at DBO.

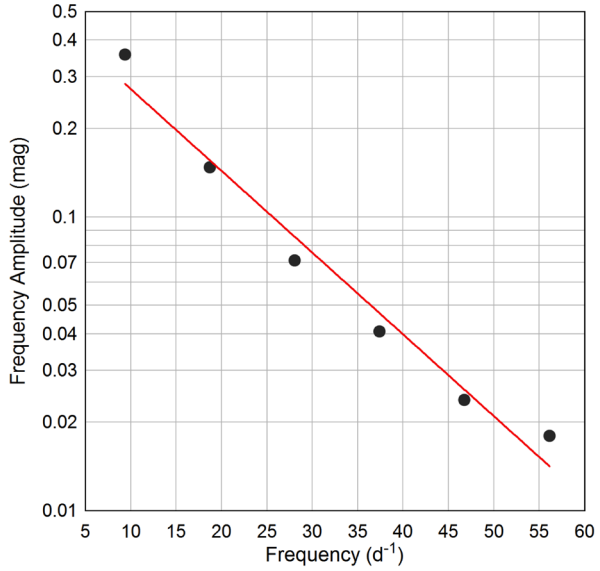

Figure 11. Amplitude decay of the fundamental (f_0) pulsation period and its corresponding partial harmonics ($2f_0$–$6f_0$) observed in the B-passband from LCs acquired in 2018 (DBO).

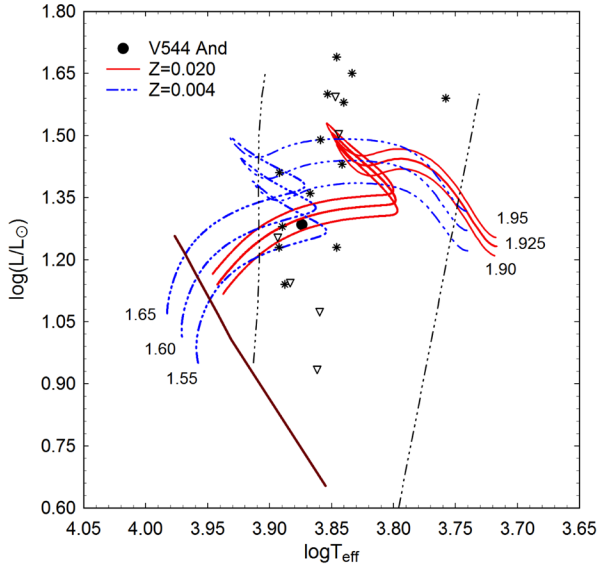

Figure 12. Evolutionary tracks (red solid lines; Z = 0.020 and blue dashed lines; Z = 0.004) derived from PARSEC models (Bressan *et al.* 2012). The position of V544 And (solid-black circle) is shown relative to ZAMS (thick maroon line) and within the theoretical instability strip (dashed lines) for low-order radial mode δ Scuti pulsators. The position of other HADS (⁕) and SX Phe (▽) variables reported by Balona (2018) are included for comparison.

3. Results and discussion

3.1. Photometry and ephemerides

Photometric values in B (n = 194), V (n = 196), and R_c (n = 198) passbands were each processed to produce LCs that spanned three days between 21 Nov and 24 Nov, 2018 (Figure 2). Period determinations were performed using PERANSO v2.6 (Paunzen and Vanmunster 2016) by applying periodic orthogonals (Schwarzenberg-Czerny 1996) to fit observations and analysis of variance to assess fit quality. In this case a mean period solution for all passbands (0.106938 ± 0.000064 d) was obtained. Folding together the sparsely sampled ROTSE-I survey data revealed a period at 0.106939 ± 0.000107 d (Figure 3). The SuperWASP survey (Butters *et al.* 2010) provided a wealth of photometric data taken (30-s exposures) at modest cadence that repeats every 9 to 12 min. These data acquired in 2006–2007 were period folded and reached superimposition when P = 0.106940 ± 0.000023 d (Figure 4). Finally, V-mag data mined from the AAVSO International Variable Star Index (2009–2018) were similarly evaluated (Figure 5) to produce a fundamental period where P = 0.106938 ± 0.000013 d. ToMax estimates were derived using the polynomial extremum fit utility featured in PERANSO 2.6 (Paunzen and Vanmunster 2016). New data derived from DBO (4), AAVSO (14), and SuperWASP (15) LCs along with published ToMax values (Table 2) were used to produce the following linear ephemeris (Equation 1):

$$\text{Max (HJD)} = 2458446.7714\,(2) + 0.1069376\,(1)\,\text{E}. \quad (1)$$

Secular changes in the fundamental period can potentially be uncovered by plotting the difference between the observed ToMax values and those predicted by the reference epoch against cycle number (Figure 6). The time difference values vs. cycle number (Table 2) are best described by a straight line relationship (Equation 1), suggesting no apparent long-term change to the fundamental period has occurred since 2004. These results along with the period folded LCs from DBO (Figure 2), ROTSE-I (Figure 3), SuperWASP (Figure 4), and AAVSO (Figure 5) also reveal that the V-mag amplitude has not changed significantly over the same period of time.

3.2. Light curve behavior

Morphologically, light curves from HADS variables are asymmetrical with rapid brightening to produce a sharply defined maximum peak. Thereafter a slower decline in magnitude results in a broad minimum. The largest difference between maximum and minimum light is observed in the blue passband (ΔB-mag = 0.88), followed by V (ΔV-mag = 0.69), and finally the smallest difference detected in infrared (ΔR_c-mag = 0.55). This behavior is characteristic of pulsating F- to A-type stars. Plotting (*B–V*) vs. phase reveals significant reddening during minimum light (Figure 7). Interstellar extinction (https://irsa.ipac.caltech.edu/applications/DUST) was obtained according to Schlafly and Finkbeiner (2011). The reddening value (E(*B–V*) = 0.0454 ± 0.0009 mag) corresponds to an intrinsic color index $(B–V)_0$ for V544 And that varies between 0.091 ± 0.036 at maximum light and 0.281 ± 0.017 mag at minimum brightness. Based on the polynomial transformation equations derived by Flower (1996), the average effective temperature (T_{eff}) was estimated to be 7853 ± 1524 K. These results based strictly on (*B–V*) photometry at DBO are higher than findings for V544 And ($T_{eff} = 7398^{+133}_{-104}$ K) included in the Gaia DR2 release of stellar parameters (Andrae *et al.* 2018). The latest data release (DR5) from the LAMOST telescope (Zhao *et al.* 2012) reports that T_{eff} = 7190 ± 18 K, wherein V544 And is assigned spectral type A7 based upon low resolution (R ≈ 1000) spectra (http://dr5.lamost.org/spectrum/view?obsid=371004085) (Rui *et al.* 2019). Parameter estimates (T_{eff}, [Fe/H], log g, and radial velocity) were derived from LAMOST DR5 using Generative Spectrum Networks following training on PHOENIX spectra (Husser *et al.* 2013). The final T_{eff} value (7480 ± 339 K) adopted for this study represents a mean value from LAMOST DR5 (7190 K), Gaia DR2 (7398 K), and DBO (7853 K).

3.3. Light curve analysis by Discrete Fourier Transformation

Discrete Fourier Transformation (DFT) was used to extract the fundamental pulsating frequency (spectral window = 100 d^{-1}) using PERIOD04 (Lenz and Breger 2005). Pre-whitening steps which successively remove the previous most intense signals were employed to tease out other potential oscillations from the residuals. Only those frequencies with a S/N ≥ 6 (Baran *et al.* 2015) in each passband are presented in Table 3. In all cases, uncertainties in frequency, amplitude, and phase were estimated by the Monte Carlo simulation (n = 400) routine featured in PERIOD04. Minor differences in the fundamental and associated harmonic frequencies between data sources (DBO vs. SuperWASP) may be attributed to decreases in the S/N ratio with harmonic order, varying filter bandpass, and/or differences in the data acquisition cadence and duration.

The DFT results demonstrate that V544 And is a monoperiodic radial pulsator; changes in stellar size during each pulsation cycle are therefore symmetrical. The amplitude spectra derived from a subset (2006–2007) of the SuperWASP data are illustrated in Figure 8. Others from DBO (B-passband) are shown in Figure 9 but do not include V- and R_c-passbands since they are essentially redundant. As would be expected, the fundamental pulsation period ($f_0 = 9.352 \pm 0.0001\ d^{-1}$) has the greatest amplitude. Sequential pre-whitening of LCs from DBO uncovered partial harmonics out as far as $6f_0$, except for the R_c-passband where detection was limited to $5f_0$. Representative DFT fits to B-, V-, and R_c-mag LC data collected at DBO (21 Nov 2018) are illustrated in Figure 10. The amplitude decay appears to be exponential as a function of harmonic order (Figure 11). This behavior has been observed with other HADS variables such as VX Hya (Templeton *et al.* 2009), RR Gem (Jurcsik *et al.* 2005), V460 And (Alton and Stępień 2019a), and V524 And (Alton and Stępień 2019b). No other independent pulsation modes were consistently detected during the short campaign at DBO or when the SuperWASP data were analyzed by PERIOD04.

3.4. Global parameters

Pulsating stars have long endured as standard candles for estimating cosmic distances ever since Henrietta Leavitt discovered a period-luminosity (P-L) relationship with

Table 3. Fundamental frequency (f_0) and corresponding partial harmonics ($2f_0$–$6f_0$) detected following DFT analysis of time-series photometric data (BVR_c) collected from V544 And at DBO (2018) along with TAMMAG2 (T) results acquired from SuperWASP (2006–2007).

	Freq. (d^{-1})	*Freq. Error*	*Amp. (mag.)*	*Amp. Error*	*Phase*	*Phase Error*	*Amp. S/N*
f_0–B	9.352	0.001	0.357	0.002	0.534	0.173	154
f_0–V	9.352	0.001	0.274	0.001	0.801	0.171	130
f_0–R_c	9.352	0.001	0.217	0.002	0.549	0.140	122
f_0–T	9.351	0.001	0.256	0.001	0.538	0.340	140
$2f_0$–B	18.706	0.001	0.148	0.002	0.252	0.172	70
$2f_0$–V	18.706	0.001	0.116	0.001	0.434	0.187	45
$2f_0$–R_c	18.707	0.001	0.094	0.001	0.738	0.159	72
$2f_0$–T	18.703	0.001	0.104	0.002	0.274	0.382	61
$3f_0$–B	28.058	0.002	0.056	0.002	0.433	0.173	41
$3f_0$–V	28.064	0.001	0.056	0.001	0.075	0.184	24
$3f_0$–R_c	28.064	0.002	0.045	0.002	0.509	0.156	32
$3f_0$–T	28.054	0.001	0.049	0.001	0.503	0.352	38
$4f_0$–B	37.401	0.003	0.041	0.002	0.030	0.182	22
$4f_0$–V	37.415	0.003	0.031	0.001	0.166	0.186	19
$4f_0$–R_c	37.072	0.004	0.023	0.002	0.057	0.151	14
$4f_0$–T	37.405	0.002	0.026	0.002	0.231	0.379	19
$5f_0$–B	46.759	0.005	0.024	0.002	0.663	0.163	10
$5f_0$–V	46.754	0.005	0.018	0.001	0.359	0.176	9
$5f_0$–R_c	46.421	0.007	0.013	0.002	0.773	0.149	11
$5f_0$–T	46.756	0.001	0.014	0.001	0.749	0.394	10
$6f_0$–B	56.132	0.007	0.018	0.002	0.329	0.179	12
$6f_0$–V	55.767	0.007	0.011	0.001	0.293	0.164	8
$6f_0$–T	56.107	0.001	0.009	0.001	0.709	0.373	7

Table 4. Global stellar parameters for V544 And using Gaia DR2 derived values and those determined directly from observations at DBO.

Parameter	*Gaia DR2*	*DBO*
Mean T_{eff} [K]	7398^{+104}_{-133}	7480 ± 339[a]
Mass [$M_\odot$]	2.00 ± 0.15	1.99 ± 0.14
Radius [$R_\odot$]	2.69 ± 0.09	2.61 ± 0.09
Luminosity [$L_\odot$]	19.56 ± 4.68	19.27 ± 5.88
$\rho_\odot$ [g/cm^3]	0.145 ± 0.018	0.157 ± 0.019
log g [cgs]	3.879 ± 0.044	3.903 ± 0.042
Q [d]	0.034 ± 0.003	0.036 ± 0.012

[a] *Value adopted is mean T_{eff} from DBO, Gaia DR2, and LAMOST DR5.*

Cepheid variables in the Small Magellanic Cloud (Leavitt and Pickering 1912). Later on, this P-L relationship was refined to accommodate differences between metal rich (Population I) and metal-poor (Population II) Cepheids (Baade 1956). Similar to Cepheids, other variable stars that pulsate via the κ-mechanism were found to obey distinct P-L relationships. P-L relationships for RR Lyrae-type variables in the mid-infrared (Neeley *et al.* 2015) and near infrared (Longmore *et al.* 1986) have been empirically-derived to estimate distances to globular clusters. A refinement of the P-L relationship for δ Sct variables was reported by McNamara (2011), albeit with now outdated Hipparcos parallaxes. A new P-L relationship using, for the most part, more accurate values determined by the Gaia Mission (Lindegren *et al.* 2016; Brown *et al.* 2018) was recently published (Ziaali *et al.* 2019). Accordingly, this empirically-derived expression (Equation 2):

$$M_V = (-2.94 \pm 0.06)\log(P) - (1.34 \pm 0.06), \quad (2)$$

is similar to the equation published by McNamara (2011) but with improved precision. The corresponding value for absolute V_{mag} ($M_V = 1.47 \pm 0.08$) when substituted into the reddening corrected distance modulus produced an estimated distance (1723 ± 78 pc) to V544 And. This result is slightly higher than the Gaia-DR2 distance (1695^{+294}_{-222} pc) but well within the confidence intervals calculated from parallax using the Bailer-Jones bias correction (Bailer-Jones 2015).

Alternatively, McNamara (2011) describes an empirical relationship (Equation 3) for metal poor stars ([Fe/H] < –2.0) where the absolute magnitude can be estimated according to:

$$M_V = (-2.90 \pm 0.05)\log(P) - (0.89 \pm 0.05). \quad (3)$$

In this case $M_V = 1.93 \pm 0.07$, so the reddening corrected distance resulted in a much lower value (1395 ± 53 pc) compared to that calculated (1723 ± 78 pc) from Equation 2. Given the uncertainty about the Gaia DR2 value (1695^{+294}_{-222} pc), which is presently considered the gold standard for distance, it is unlikely that these values are statistically different.

The location of V544 And, which is ~682 pc below the Galactic plane, suggests residence in the thick disc where the scale height is ~0.9 kpc (Li and Zhao 2017) rather than the halo where many metal poor ([Fe/H] < –1.6) stars reside (Carollo *et al.* 2010). The proper motion ($\mu_\alpha = 17.873 \pm 0.101$; $\mu_\delta = -8.304 \pm 0.174$ km·s^{-1}) and distance (1695 pc) to V544 And are known from Gaia DR2 (Lindegren *et al.* 2016; Brown *et al.* 2018) while the radial velocity ($v_R = -15.3 \pm 7.1$ km·s^{-1}) has been reported in LAMOST DR5 (Rui *et al.* 2019). Space velocities (($U_{LSR} = -81.7$, $V_{LSR} = -122.4$, and $W_{LSR} = -16.9$ km·s^{-1}) were determined (http://kinematics.bdnyc.org/query) relative to the local standard of rest assuming the solar motion reported by Dehnen and Binney (1998) where U = 10, V = 5.3, and W = 7.2 km·s^{-1}. More recent (Coşkunoğlu *et al.* 2011) estimates for the solar motion standard of rest (U = –8.5, V = 13.38, and W = 6.49 km·s^{-1}) lead to somewhat different space velocities for V544 And ($U_{LSR} = 93.02$, $V_{LSR} = -104.32$, and $W_{LSR} = -23.75$ km·s^{-1}) (https://rdrr.io/cran/astrolibR/man/gal_uvw.html). However, other than a change in convention where U_{LSR} is positive outward toward the Galactic anticenter, total spatial velocity

$$\left(\sqrt{U^2_{LSR} + V^2_{LSR} + W^2_{LSR}}\right)$$

by either local standard of rest is too small (≤ 148.1 km·s^{-1}) for a halo object (> 180 km·s^{-1}) but convincingly within the range for a thick disk resident (Yan *et al.* 2019).

Gaia DR2 also includes estimates for solar radius and luminosity (Andrae *et al.* 2018). In this regard it is worth noting that there are some differences in the equations used to produce the Gaia DR2 values reported for V544 And and those otherwise determined herein (Table 4). The corresponding data reduction has been discussed in more detail for two other HADS variables V460 And (Alton and Stępień 2019a) and V524 And (Alton and Stępień 2019b).

The mass of a single isolated field star is very difficult to determine directly. Instead, a mass-luminosity (M-L)

relationship ($1.05 < M/M_{\odot} \leq 2.40$) developed by Eker *et al.* (2018) for main sequence (MS) stars in detached binary systems was used as the best estimate. This expression (Equation 4):

$$\log(L) = 4.329(\pm 0.087) \cdot \log(M) - 0.010(\pm 0.019), \quad (4)$$

leads to a mass (2.00 ± 0.15) in solar units as derived from the Gaia DR2 stellar parameters where $L = 19.56 \pm 4.68\ L_{\odot}$. All values summarized in Table 4 fall well within expectations for a HADS variable. It should be emphasized that these fundamental physical parameters were derived by assuming a null value for the Gaia extinction ($A_G = 0$). V544 And resides in a region of the Milky Way (Gal. coord. (J2000): $l = 134.3183$; $b = -23.7149$) where the interstellar extinction ($A_V = 0.1417 \pm 0.0028$) is measureably different from zero (Schlafly and Finkbeiner 2011). Therefore, the same equations (Equations 6–8 in Alton and Stępień 2019a) were applied but this time using the data obtained at DBO where $V_{avg} = 12.790 \pm 0.023$, $A_V = 0.1417 \pm 0.0028$, $M_V = 1.528$, $T_{eff} = 7480$ K, and $BC_V = 0.0243$. The results summarized in Table 4 indicate that the Gaia DR2 reported values for luminosity and radius appear to be comparable even with different assumptions about interstellar extinction. The luminosity ($19.27 \pm 5.88\ L_{\odot}$) produced from the DBO data translates into a radius ($R_* = 2.61 \pm 0.09$) and a mass of 1.99 ± 0.141. Additionally, stellar radius in solar units was independently determined from an empirically derived period-radius (P-R) relationship (Equation 5) reported by Laney *et al.* (2003) for HADS and classical Cepheids:

$$\log(R_*) = a + b \cdot \log(P) + c, \quad (5)$$

where $a = 1.106 \pm 0.012$, $b = 0.725 \pm 0.010$, and $c = 0.029 \pm 0.024$. In this case the value for R_* ($2.70 \pm 0.40\ R_{\odot}$) was closer to the value obtained from the Gaia DR2 estimates ($2.69 \pm 0.09\ R_{\odot}$). Khruslov (2008) suggested the "large distances from the Galactic plane make it possible to consider" classifying V544 And as an SX Phe-type pulsator. However, as mentioned earlier, more recent distance and kinematic evidence suggests that V544 And does not inhabit the halo where metal deficient ([Fe/H] < –1.6) stars typically reside. Moreover, the mass threshold of an SX Phe-type variable is generally regarded to be less than 1.3 $M_{\odot}$ (McNamara 2011). This significant distinction challenges the notion that V544 And is an SX Phe-type variable.

Derived values for density ($\rho_{\odot}$), surface gravity (log g), and pulsation constant (Q) are also included in Table 4. Stellar density (ρ_*) in solar units (g/cm^3) was calculated according to Equation 6:

$$\rho_* = 3 \cdot G \cdot M_* \cdot m_{\odot} / (4\pi (R_* \cdot r_{\odot})^3). \quad (6)$$

where G is the cgs gravitational constant, $m_{\odot}$ = solar mass (g), $r_{\odot}$ = solar radius (cm), M_* is the mass, and R_* the radius of V544 And, both in solar units. Using the same algebraic assignments, surface gravity (log g) was determined by the following expression (Equation 7):

$$\log g = \log (M_* \cdot m_{\odot} / (R_* \cdot r_{\odot})^2). \quad (7)$$

The dynamical time that it takes a p-mode acoustic wave to internally traverse a star is related to its size but more strongly correlates to the stellar mean density. The pulsation constant (Q) is defined by the period-density relationship (Equation 8):

$$Q = P \sqrt{\bar{\rho}_* / \bar{\rho}_{\odot}}\ . \quad (8)$$

where P is the pulsation period (d) and $\bar{\rho}_*$ and $\bar{\rho}_{\odot}$ are the mean densities of the target star and Sun, respectively. The mean density can be expressed (Equation 9) in terms of other measurable stellar parameters where:

$$\log(Q) = -6.545 + \log(P) + 0.5 \log(g) + 0.1\, M_{bol} + \log(T_{eff}). \quad (9)$$

The full derivation of this expression can be found in Breger (1990). The resulting Q value (Table 4) derived from observations at DBO is consistent with theory and the distribution of Q-values (0.03–0.04 d) from fundamental radial pulsations observed with other δ Sct variables (Breger 1979; Joshi and Joschi 2015; Antonello and Pastori 1981).

3.5. Evolutionary status of V544 And

The evolutionary status of V544 And was evaluated (Figure 12) using PARSEC-derived stellar tracks and isochrones (Bressan *et al.* 2012) and then plotted ($\log T_{eff}$ vs. $\log(L/L_{\odot})$) as a theoretical Hertzsprung-Russell diagram (HRD). The thick solid maroon-colored line defines the zero-age main sequence (ZAMS) position for stars with metallicity $Z = 0.014$. The two broken lines nearly perpendicular to the ZAMS delimit the blue (left) and red (right) edges of the theoretical instability strip for radial low-p modes (Xiong *et al.* 2016). Included are the positions of several known HADS and SX Phe-type variables (Balona 2018). The solid-black circle indicates the position of V544 And using the DBO derived parameters and corresponding error estimates provided in Table 4. Over the last few decades, the reference metallicity values used by several authors for computing stellar models have ranged between 0.012 and 0.020 (Amard *et al.* 2019). Investigations focused on a definitive value for $Z_{\odot}$ have been recently reported (von Steiger and Zurbuchen 2016; Serenelli *et al.* 2016; Vagnozzi *et al.* 2017); ironically a single undisputed value for solar metallicity remains elusive. Nonetheless, a metal abundance (Z) value is required in order to determine the mass, radius, and age of V544 And from theoretical evolutionary tracks. A Z-value can be estimated indirectly from its Galactic coordinates and kinematic properties. As mentioned earlier, the total spatial velocity (148.1 $km \cdot s^{-1}$) suggests affiliation with the galactic thick disc (Yan *et al.* 2019). Its distance from the galactic plane (–682 pc) also favors a thick disc membership rather than residence in the halo. It can therefore be assumed that V544 And approaches solar metallicity, or at most a few times lower.

Two separate PARSEC evolutionary models (Bressan *et al.* 2012) each ranging in age between 1×10^8 and 1.7×10^9 y are illustrated in Figure 12. The red solid lines show the models ($M_{\odot} = 1.90$, 1.925, and 1.95) when $Z = 0.020$, while the blue, dash-dotted lines define the models ($M_{\odot} = 1.55$, 1.60, and 1.65) where $Z = 0.004$. The latter simulations correspond to a decrease in metallicity by a factor of 3 to 5 depending on the reference

solar metallicity. Assuming Z = 0.020, it can be seen that V544 And would have a mass of $1.91 \pm 0.02\ M_{\odot}$ and a radius of $2.69 \pm 0.13\ R_{\odot}$. The position of this intrinsic variable along the $M_{\odot}$=1.90 evolutionary track corresponds to an age of 1.09 Gyr suggesting it is a moderately evolved MS object lying amongst other HADs close to the blue edge of the instability strip.

By comparison, if V544 And is a metal poor (Z = 0.004) star, then it would have a similar radius (2.51 ± 0.20), but would be less massive ($1.58\ M_{\odot}$). Its position lies just prior to the HRD region where evolutionary tracks of low metallicity stars begin stellar contraction near the end of hydrogen burning in the core. This star would still be a MS object but with an age approaching 1.50 Gyr.

The theoretical mass ($1.91\ M_{\odot}$) where Z = 0.020 favors the higher metallicity of V544 And and is in good agreement with results independently determined (Table 4) using an empirical M-L relationship. In this regard, the LAMOST DR5 metallicity value ([Fe/H] = –0.571) may be underestimated or does not scale with its total metal abundance (Z). By any measure, V544 And is very likely not a metal poor ([Fe/H] < –1) star traditionally associated with SX Phe-type variables. Should high resolution spectroscopic data become available in the future, uncertainty about the mass of V544 And will likely improve.

4. Conclusions

This first multi-color (BVR_c) CCD study of V544 And has produced 4 new times-of-maximum along with another 29 values culled from the SuperWASP survey and the AAVSO archives. These results and other published values resulted in a new linear ephemeris. An assessment using the observed and predicted times-of-maximum suggests that since 2004 very little change in the fundamental pulsation period has occurred and that the V-mag amplitude has not changed significantly over the same period of time. Deconvolution of time-series photometric data by discrete Fourier transformation shows that V544 And is a monoperiodic radial pulsator ($f_0 = 9.352\ d^{-1}$) which also oscillates in at least five other partial harmonics ($2f_0 - 6f_0$). A mean effective temperature for V544 And (7480 ± 339 K) was estimated from LAMOST DR5, Gaia DR2, and DBO results and corresponds to spectral type A7. These results, along with the distance (1724 ± 78 pc) estimated from the distance modulus, agreed reasonably well with the same findings (1695^{+294}_{-222} pc) provided in Gaia DR2. The pulsation period (~0.10694 d), radial oscillation mode, V_{mag} amplitude (0.69 mag), and LC morphology are all consistent with the defining characteristics of a HADS variable. However, these three parameters do not necessarily exclude the possibility that V544 And is a field SX Phe-type pulsator. Nonetheless in this case, the estimated mass of V544 And (~1.9–2 $M_{\odot}$) far exceeds the generally accepted threshold ($M < 1.3\ M_{\odot}$) for SX Phe stars (McNamara 2011). Moreover, evolutionary tracks from the PARSEC model which assume near solar abundance (Z = 0.020) are best matched by a MS star with a mass of 1.91 $M_{\odot}$ and radius of 2.69 $R_{\odot}$. Finally there is a high probability that V544 And resides in the thick disk based on total spatial velocity. Given these results, the weight of evidence indicates that V544 And should be classified as a HADS rather than an SX Phe variable.

5. Acknowledgements

This research has made use of the SIMBAD database operated at Centre de Données astronomiques de Strasbourg, France. Time-of-maximum light data from the Information Bulletin on Variable Stars (IBVS) website proved invaluable to the assessment of potential period changes experienced by this variable star. In addition, the Northern Sky Variability Survey hosted by the Los Alamos National Laboratory and the International Variable Star Index archives maintained by the AAVSO were mined for critical information. This work also presents results from the European Space Agency (ESA) space mission Gaia. Gaia data are being processed by the Gaia Data Processing and Analysis Consortium (DPAC). Funding for the DPAC is provided by national institutions, in particular the institutions participating in the Gaia MultiLateral Agreement (MLA). The Gaia mission website is https://www.cosmos.esa.int/gaia. The Gaia archive website is https://archives.esac.esa.int/gaia. This paper makes use of data from the first public release of the WASP data as provided by the WASP consortium and services at the NASA Exoplanet Archive, which is operated by the California Institute of Technology, under contract with the National Aeronautics and Space Administration under the Exoplanet Exploration Program. The use of public data from LAMOST is also acknowledged. Guoshoujing Telescope (the Large Sky Area Multi-Object Fiber Spectroscopic Telescope LAMOST) is a National Major Scientific Project built by the Chinese Academy of Sciences. Funding for the project has been provided by the National Development and Reform Commission. LAMOST is operated and managed by the National Astronomical Observatories, Chinese Academy of Sciences. The thoughtful guidance provided by Professor K. Stępień during is much appreciated while the careful review and helpful commentary provided by an anonymous referee is gratefully acknowledged.

References

Akerlof, C., *et al.* 2000, *Astron. J.*, **119**, 1901.

Alton, K. B., and Stępień, K. 2019a, *J. Amer. Assoc. Var Star Obs.*, **47**, 53.

Alton, K. B., and Stępień, K. 2019b, *Acta Astron.*, **69**, 283.

Amard, L., Palacios, A., Charbonnel, C., Gallet, F., Georgy, C., Lagarde, N., and Siess, L. 2019, *Astron. Astrophys.*, **631A**, 77.

Andrae, R., *et al.* 2018, *Astron. Astrophys.*, **616A**, 8.

Antonello, E., and Pastori, L. 1981, *Publ. Astron. Soc. Pacifc*, **93**, 237.

Baade, W. 1956, *Publ. Astron. Soc. Pacifc*, **68**, 5.

Baglin, A. 2003, *Adv. Space Res.*, **31**, 345.

Bailer-Jones, C. A. L. 2015, *Publ. Astron. Soc. Pacifc*, **127**, 994.

Balona, L. A. 2018, *Mon. Not. Roy. Astron. Soc.*, **479**, 183.

Balona, L. A., and Nemec, J. M. 2012, *Mon. Not. Roy. Astron. Soc.*, **426**, 2413.

Baran, A. S., Koen, C., and Pokrzywka, B. 2015, *Mon. Not. Roy. Astron. Soc.*, **448**, L16.

Berry, R., and Burnell, J. 2005, *The Handbook of Astronomical Image Processing*, 2nd ed., Willmann-Bell, Richmond VA.

Breger, M. 1979, *Publ. Astron. Soc. Pacifc*, **91**, 5.
Breger, M. 1990, *Delta Scuti Star Newsl.*, **2**, 13.
Bressan, A., Marigo, P., Girardi, L., Salasnich, B., Dal Cero, C., Rubele, S., and Nanni, A. 2012, *Mon. Not. Roy. Astron. Soc.*, **427**, 127.
Brown, A. G. A., *et al.* 2018, *Astron. Astrophys.*, **616A**, 1.
Butters, O. W., *et al.* 2010, *Astron. Astrophys.*, **520**, L10.
Carollo, D., *et al.* 2010, *Astrophys. J.*, **712**, 692.
Coşkunoğlu, *et al.* 2011, *Mon. Not. Roy. Astron. Soc.*, **412**, 1237.
Dehnen, W., and Binney, J. J. 1998, *Mon. Not. Roy. Astron. Soc.*, **298**, 387.
Eker, Z., *et al.* 2018, *Mon. Not. Roy. Astron. Soc.*, **479**, 5491.
Flower, P. J. 1996, *Astrophys. J.*, **469**, 355.
Garg, A., *et al.* 2010, *Astron. J.*, **140**, 328.
Gilliland, R. L., *et al.* 2010, *Publ. Astron. Soc. Pacifc*, **122**, 131.
Hűbscher, J. 2015, *Inf. Bull. Var. Stars*, No. 6152, 1.
Husser, T.-O., Wende-von Berg, S., Dreizler, S., Homeier, D., Reiners, A., Barman, T., and Hauschildt, P. H. 2013, *Astron. Astrophys.*, **553A**, 6.
Joshi, S., and Joshi, Y. C. 2015, *J. Astrophys. Astron.*, **36**, 33.
Jurcsik, J., *et al.* 2005, *Astron. Astrophys.*, **430**, 1049.
Kafka, S. 2019, variable star observations from the AAVSO International Database (https://www.aavso.org/aavso-international-database).
Khruslov, A. V. 2008, *Peremennye Zvezdy Prilozhenie*, **8**, 5.
Laney, C. D., Joner, M., and Rodriguez, E. 2003, in *Interplay of Periodic, Cyclic and Stochastic Variability in Selected Areas of the H-R Diagram*, ed. C. Sterken, ASP Conf. Ser. 292, Astronomical Society of the Pacific, San Francisco, 203.
Leavitt, H. S., and Pickering, E. C. 1912, *Harvard Coll. Obs. Circ.*, No. 173, 1.
Lee, Y.-H., Kim, S. S., Shin, J., Lee, J., and Jin, H. 2008, *Pub. Astron. Soc. Japan*, **60**, 551.
Lenz, P., and Breger, M. 2005, *Commun. Asteroseismology*, **146**, 53.
Li, C. and Zhou, G. 2017, *Astrophys. J.*, 850, 25.
Lindegren, L., *et al.* 2016, *Astron. Astrophys.*, **595A**, 4.
Longmore, A. J., Fernley, J. A., and Jameson, R. F. 1986, *Mon. Not. Roy. Astron. Soc.*, **220**, 279.
McNamara, D. H. 2000, in *Delta Scuti and Related Stars, Reference Handbook and Proceedings of the 6th Vienna Workshop in Astrophysics*, ed. M. Breger, M. Montgomery, ASP Conf. Ser. 210, Astronomical Society of the Pacific, San Francisco, 373.
McNamara, D. H. 2011, *Astron. J.*, **142**, 110.
Minor Planet Observer. 2019, MPO Software Suite (http://www.minorplanetobserver.com), BDW Publishing, Colorado Springs.
Neeley, J. R., *et al.* 2015, *Astrophys. J.*, **808**, 11.
Niu, J.-S., Fu, J.-N., and Zong, W.-K. 2013, *Res. Astron. Astrophys.*, **13**, 1181.
Niu, J.-S., *et al.* 2017, *Mon. Not. Roy. Astron. Soc.*, **467**, 3122.
Pamyatnykh, A. A., Handler, G., and Dziembowski, W. A. 2004, *Mon. Not. Roy. Astron. Soc.*, **350**, 1022.
Paunzen, E., and Vanmunster, T. 2016, *Astron. Nachr.*, **337**, 239.
Poretti, E. 2003a, *Astron. Astrophys.*, **409**, 1031.
Poretti, E. 2003b, in *Interplay of Periodic, Cyclic and Stochastic Variability in Selected Areas of the H-R Diagram*, ed. C. Sterken, ASP Conf. Ser. 292, Astronomical Society of the Pacific, San Francisco, 145.
Rui, W., *et al.* 2019, *Pub. Astron. Soc. Pacifc*, **131**, 024505.
Schlay, E. F., and Finkbeiner, D. P. 2011, *Astrophys. J.*, **737**, 103.
Schwarzenberg-Czerny, A. 1996, *Astrophys. J., Lett.*, **460**, L107.
Serenelli, A., Scott, P., Villante, F. L., Vincent, A. C., Asplund, M., Basu, S., Grevesse, N., and Peña-Garay, C. 2016, *Mon. Not. Roy. Astron. Soc.*, **463**, 2.
Software Bisque. 2019, THESKYX PRO imaging software (http://www.bisque.com).
Templeton, M. R., Samoly, G., and Dvorak, S. 2009, *Pub. Astron. Soc. Pacifc*, **121**, 1076.
Vagnozzi, S., Freese, K., and Zurbuchen, T. H. 2017, *Astrophys. J.*, **839**, 55.
von Steiger, R., and Zurbuchen, T. H. 2016, *Astrophys. J.*, **816**, 13.
Walker, G., *et al.* 2003, *Publ. Astron. Soc. Pacifc*, **115**, 1023.
Warner, B. D. 2007, *Minor Planet Bull.*, **34**, 113.
Watson, C., Henden, A. A., and Price, C. A. 2014, AAVSO International Variable Star Index VSX (Watson+, 2006–2014; http://www.aavso.org/vsx).
Wils, P., *et al.* 2011, *Inf. Bull. Var. Stars*, No. 5977, 1.
Wils, P., *et al.* 2012, *Inf. Bull. Var. Stars*, No. 6015, 1.
Wils, P., *et al.* 2013, *Inf. Bull. Var. Stars*, No. 6049, 1.
Wils, P., *et al.* 2014, *Inf. Bull. Var. Stars*, No. 6122, 1.
Wils, P., *et al.* 2015, *Inf. Bull. Var. Stars*, No. 6150, 1.
Wozniak, P. R., *et al.* 2004, *Astron. J.*, **127**, 2436.
Xiong, D. R., Deng, L., Zhang, C., and Wang, K. 2016, *Mon. Not. Roy. Astron. Soc.*, **457**, 3163.
Yan, Y., Du, C., Liu, S., Li, H., Shi, J., Chen, Y., Ma, J., and Wu, Z. 2019, *Astrophys. J.*, **880**, 36.
Zhao, G., Zhao, Y.-H., Chu, Y.-Q., Jing, Y.-P, and Deng, L.-C. 2012, *Res. Astron. Astrophys.*, **12**, 723.
Ziaali, E., Bedding, T. R., Murphy, S. J., Van Reeth, T., and Hey, D. R. 2019, *Mon. Not. Roy. Astron. Soc.*, **486**, 4348.